Hemispheric Asymmetry of Phase Partition in Mixed-Phase Clouds Based on Near Global-Scale Airborne Observations

Ching An Yang[1,2], Minghui Diao[1,*], Yang Shi[3,4,5], Xiaohong Liu[3]

[1]Department of Meteorology and Climate Science, San Jose State University, San Jose, CA, USA
[2]*Current affiliation:* Climate and Space Sciences and Engineering, University of Michigan, Ann Arbor, MI, USA
[3]Department of Atmospheric Sciences, Texas A&M University, College Station, TX, USA
[4]Department of Civil Environmental Engineering, Massachusetts Institute of Technology, Cambridge, MA
[5]*Current affiliation:* Atmospheric, Climate, & Earth Sciences Division, Pacific Northwest National Laboratory, Richland, WA, USA

*Corresponding author:
Minghui Diao, Ph.D., Professor
Minghui.diao@sjsu.edu

Key Points

- Southern Hemisphere has higher occurrence frequency and higher mass fraction of supercooled liquid water than Northern Hemisphere
- E3SMv1/EAMv1 model misses the hemispheric asymmetry of phase partition listed above
- LWC is consistently too high in EAMv1 in all phases, but IWC biases depend on cloud phase

Abstract

Mixed-phase clouds contribute to substantial uncertainties in global climate models due to their complex microphysical properties. Former model evaluations almost exclusively rely on satellite observations to assess cloud phase distributions globally. This study investigated mixed-phase cloud properties using near global-scale *in situ* observation datasets from 14 flight campaigns in combination with collocated output from a global climate model. The Southern Hemisphere (SH) shows significantly higher occurrence frequencies and higher mass fractions of supercooled liquid water than Northern Hemisphere (NH) based on observations at 0.2 and 100 km horizontal scales. Such hemispheric asymmetry is not captured by the model. The model also consistently overestimates liquid water content (LWC) in all cloud phases but shows ice water content (IWC) biases that vary with phase. Key processes contributing to model biases in phase partition can be identified through the combination of evaluation of phase frequency, liquid mass fraction, LWC and IWC.

Plain Language Summary

The partition between supercooled liquid water and ice in clouds affects how clouds interact with solar and terrestrial radiation. Mixed-phase clouds, which may contain both supercooled liquid droplets and ice crystals, are especially challenging for climate models to represent. This study compares the occurrence frequencies and microphysical properties of these clouds between the Northern and Southern Hemispheres using data from multiple aircraft-based field campaigns and simulations from a global climate model. The Southern Hemisphere shows higher probabilities of liquid clouds and higher mass fractions of supercooled liquid water than the Northern Hemisphere.

These hemispheric differences are not captured by the model. The results indicate that mixed-phase clouds may have different responses to a changing global climate in the two hemispheres.

1. Introduction

Clouds represent a crucial component of the Earth system due to their modulations of energy transfer and radiative balance (e.g. Hartmann et al., 1992; Matus and L'Ecuyer, 2017). In the temperature range of -35° – 0°C (hereafter defined as the mixed phase cloud regime), ice crystals and supercooled liquid droplets can potentially co-exist. These clouds demonstrate large spatial heterogeneities in their macrophysical properties (e.g., genuinely mixed or conditionally mixed ice and liquid segments, Korelev et al., 2017; Korolev and Milbrandt, 2022) and microphysical properties (e.g., partition between ice crystals and supercooled liquid droplets, Maciel et al., 2024). These spatial heterogeneities impose a challenge to various types of observational techniques (D'Alessandro et al., 2023; Wang et al., 2024) as well as the parameterizations at sub-grid scales in global climate models (GCMs) (Zhang et al., 2019; Zhang et al., 2024).

Traditionally, satellite observations have been the gold standard for quantifying the frequency distributions of three cloud thermodynamic phases – liquid, ice, and mixed phases – at a near global scale (e.g., Hu et al., 2010; Cesana & Chepfer, 2012; Sokol & Storelvmo, 2024). Satellite observations have also been proven highly valuable for the evaluation of mixed-phase clouds in GCM simulations (Kay et al., 2016; Tan & Storelvmo, 2016; Cesana et al., 2022; Hofer et al., 2024). Phase partition between ice and supercooled liquid water has been found to play an important role in the estimations of climate feedback and climate sensitivity (e.g., Tan et al., 2016; Frey & Kay, 2017; McCoy et al., 2017; Zelinka et al., 2020). However, inherent issues still exist in the spaceborne retrievals of mixed-phase cloud regime, such as the attenuation of lidar signals when penetrating through supercooled liquid-topped cloud layers (e.g., Silber et al., 2018; Desai et al., 2023; Wang et al., 2024) and the large uncertainties in the derivations of hydrometeor concentrations (e.g., Hogan et al., 2005). When comparing three satellite-derived cloud phase products with *in situ* airborne observations, statistically significant discrepancies were seen at various latitudes and pressure levels (Wang et al., 2024). These remaining challenges in spaceborne observations demonstrate the need of conducting an alternate type of analysis of cloud phases at global scales to complement the conventional satellite-based analysis.

This study presents an alternative approach for investigations of cloud phase distributions and microphysical properties at a near global scale based on *in situ* airborne observations from multiple flight campaigns. As far as the authors are aware, a hemispheric comparison for cloud phase partition has not been conducted previously based on *in situ* airborne observations, nor has an evaluation study of GCM simulations been conducted against *in situ* observations at a near pole-to-pole scale (i.e., 75°S to 87°N). By leveraging the compiled *in situ* observation dataset, this study is uniquely poised to examine mixed-phase cloud properties that could be challenging to derive from remote sensing retrievals, including the frequency distributions of three thermodynamic phases at various temperatures (Section 3.1), the partition between liquid and ice at various latitudes (Section 3.2), and cloud microphysical properties, i.e., ice water content (IWC) and liquid water content (LWC), for each cloud phase (Section 3.3).

2. Methodology

2.1 *In situ* datasets and instrumentation

This study compiled observation datasets of eleven U.S. National Science Foundation (NSF) and three U.S. Department of Energy (DOE) airborne campaigns, including NSF START08 (Pan et al., 2010), HIPPO (Wofsy, 2011), PREDICT (Montgomery et al., 2012), TORERO (Volkamer et al., 2015), DC3 (Barth et al., 2015), CONTRAST (Pan et al., 2017), WINTER (Lee et al., 2018), CSET (Albrecht et al., 2019), ORCAS (Stephens et al., 2018), SOCRATES (McFarquhar et al., 2021), and OTREC (Fuchs-Stone et al., 2020) campaigns, as well as DOE M-PACE (Verlinde et al., 2007), ISDAC (McFarquhar et al., 2011), and ACME-V (Maahn et al., 2017) campaigns. Supplementary Table S1 provides detailed information about these campaigns, including name, number of research flights, time, location, and flight hours at all temperatures as well as at mixed-phase range. A total of 576 hours were flown at -35°C to 0°C, with 463 and 113 hours of clear-sky and in-cloud conditions, respectively. Collectively, the 14 airborne campaigns conducted between April 2008 and September 2019 covered a spatial range from 75°S to 87°N and from 38°W to 128°E (Figure 1 a). A similar but smaller *in situ* observation dataset was previously used in Wang et al. (2024) as described in their Table 1 to validate three satellite-based cloud phase products.

For most campaigns (except M-PACE and ISDAC), we applied a phase identification method that involves (i) the identification of ice or supercooled liquid for each second of a cloud probe and (ii) IWC and LWC calculations (D'Alessandro et al., 2019; Yang et al., 2021; Maciel et al., 2024). Several key parameters were used, including the mass–number concentration (M–N) relationship, maximum particle diameters, the standard deviations of particle size distributions, and temperature. For most campaigns, these parameters were derived from the Cloud Droplet Probe (CDP) (2–50 μm) and the Fast-Two Dimensional Cloud probe (Fast-2DC) (62.5–3200 μm). The 2-Dimensional Stereo (2DS) cloud probe (40 – 5000 μm) was used instead of the Fast-2DC probe in SOCRATES and ACME-V. The 1-Hz CDP observations were categorized as large aerosols ($N \le 10^{-1.5}$ cm^{-3} or $M \le 10^{-3.4}$ g m^{-3}), ice crystals (both $10^{-1.5} < N < 10^{-0.5}$ cm^{-3} and $M > 10^{-3.4}$ g m^{-3}), or liquid droplets (both $N \ge 10^{-0.5}$ cm^{-3} and $M > 10^{-3.4}$ g m^{-3}). A more complex decision tree was applied for Fast-2DC and 2DS following D'Alessandro et al. (2019).

To calculate LWC or IWC, spherical shape was assumed for supercooled liquid droplets, while the mass-dimension (M-D) relationships from Brown and Francis (1995) were used for small and large ice particles, separated by maximum dimensions ≤ and > 75 μm, respectively. M-PACE (McFarquhar et al., 2007) and ISDAC (Jackson et al., 2012) derived IWC and LWC from two different suites of instruments. M-PACE used Forward Scattering Spectrometer Probe (FSSP), 1-Dimensional Cloud probe (1DC), 2DC, and High Volume Precipitation Spectrometer (HVPS), while ISDAC used FSSP, CDP, 2DC, 2DS, Cloud Imaging Probe 2 (CIP2), and 2-D Precipitation (2DP) probe.

A consistent definition of three cloud phases was applied to all observations and simulations. That is, if supercooled liquid fraction (SLF) < 0.1, between 0.1 – 0.9, or > 0.9, then this sample is defined as ice, mixed, or liquid phase, respectively. Here SLF = LWC / (LWC + IWC), which represents the mass fraction of supercooled liquid water.

2.2 Model Simulations

The DOE Energy Exascale Earth System Models version 1 (E3SMv1), specifically its atmospheric component, the E3SM Atmosphere Model version 1 (EAMv1), was used in this work (Xie et al., 2018; Rasch et al., 2019). EAMv1 employs a Spectral Element (SE) dynamical core at ~1-degree resolution with 72 vertical levels (Golaz et al., 2019). The SE dynamical core uses unstructured grids and has advantages of near-perfect scalability and GPU (Graphics Processing

Unit) acceleration (Dennis et al., 2012; Adbi et al., 2017). Cloud microphysics in EAMv1 are treated by version 2 of Morrison and Gettelman (MG2) with representations of cloud particle formation, growth, and precipitation processes (Gettelman et al., 2015). Cloud macrophysics, shallow convection, and boundary layer turbulence are simulated using the Cloud Layers Unified By Binormals (CLUBB) (Golaz et al., 2002; Larson & Golaz, 2005), deep convection processes are parameterized based on Zhang and McFarlane (1995), and the aerosol module used the Modal Aerosol Module (MAM4) (Liu et al., 2016).

For each flight campaign, one model simulation was set up to cover the same time period with ~6 months of spin-up time prior to the start date of the campaign. The model output was saved along the flight tracks at a 10-minute frequency. Simulations were nudged towards the Modern-Era Retrospective Analysis for Research and Applications, Version 2 (MERRA-2) reanalysis dataset (Gelaro et al., 2017) for temperature and horizontal wind fields, consistent with previous model evaluation studies (e.g., Yang et al., 2021; Yip et al., 2021; Patnaude et al., 2024; Desai et al., 2023, 2025). Several sensitivity tests were conducted to examine the impacts of vertical sampling and horizontal spatial averaging, similar to the method used in Yang et al. (2021) in their section 2.3, and consistent results were found among these tests.

3. Results

3.1 Cloud phase frequency distributions and phase partition at a near global scale

One advantage of airborne observations is the ability to provide synchronized *in situ* measurements of cloud hydrometeors and environmental conditions (such as temperature). Hence, the mass partition between supercooled liquid and ice (indicated by SLF) is examined as a function of temperature in two hemispheres (Figure 1 b and 1 c), with the number of samples shown in Figure S1. As for seasonal distributions, most samples in the SH occurred during austral summer, while the NH has more similar sample sizes in all four seasons (Table S2 and Figure S2).

Based on high-resolution 1-s observations, a main hemispheric difference is the higher SLF in the SH compared with the NH, with SLF in the SH being 0.2 – 0.4 higher at -25 to 0°C. A moving average at 100-km resolution that included both clear-sky and in-cloud segments was used to compare with model grid-mean values, consistent with the method used in D'Alessandro et al. (2019) and Yang et al. (2021). After spatial averaging, SLF shows larger increases in the NH (by 0.1 – 0.2) than the SH (by 0.05 – 0.1), because the 1-s observations are dominated by pure ice segments especially in the NH, while 100-km observations have more mixtures of ice and liquid.

Compared with the 100-km observations, the EAMv1 simulations show similar SLF values in the SH but show much higher SLF in the NH by 0.1 – 0.2. Consequently, the EAMv1 simulations do not show a significant contrast of SLF between the two hemispheres. This result indicates that future improvement of the model parameterization should convert more liquid-containing clouds to the ice-containing clouds at temperatures between -35°C to 0°C in the NH.

3.2 Latitudinal-temperature distributions of three cloud phases

The latitudinal-temperature distributions of three cloud phases are shown in Figure 2. The number of samples and in-cloud frequencies are shown in Figures S3 and S4, respectively. To reduce the noise in frequency distributions due to fluctuations of sampling sizes, we applied an averaging process to every 3×3 bins (i.e., a center bin and its 8 surrounding bins). Key features are consistently seen without the 3×3 grid smoothing (Figure S5) or using a larger model sample size (Figure S6). The cloud phase frequency is calculated as the number of a phase divided by the total number of in-cloud samples in each bin. In addition, in-cloud frequency is calculated as the number of in-cloud samples divided by the total number of all-sky samples.

A hemispheric contrast is consistently seen in this latitudinal view based on *in situ* observations at both ~0.2-km and 100-km resolutions, showing higher liquid phase frequency in the SH compared with the NH (Figure 2 a and 2 b). The EAMv1 simulations show similar latitudinal gradient of in-cloud frequencies compared with 100-km observations, with the highest in-cloud frequencies located at the polar regions (Figure S4). However, the lack of hemispheric differences in frequency distributions of liquid and ice phases is seen in the simulations, consistent with the lack of hemispheric asymmetry in SLF (Figure 1).

The hemispheric differences for observations and simulations are more evidently represented in Figure 3, including the differences between each pair of latitudinal-temperature bins symmetrically distributed between the NH and SH (columns 1 – 4) and the phase occurrence frequencies in each 5°C temperature bin (column 4). The number of samples are shown in Figure S7. Both 1-s and 100-km observations show higher liquid phase frequency in the SH by 0.2 to 0.4 than the NH at -25 to 0°C (Figure 3 d). Such observed hemispheric differences are even larger at higher temperatures than lower temperatures. In addition, both observations show significantly higher ice phase frequencies in the extratropical regions in the NH (> 30°N) compared with the extratropics in the SH (< 30°S) (Figure 3 i and 3 j).

The model simulations show lack of hemispheric differences in both liquid and ice phase frequencies (Figure 3 d and 3 l). These lack of hemispheric differences in the simulations can be attributed to the different magnitudes of model biases between the two hemispheres for liquid and ice frequencies. That is, simulations in the SH show similar liquid and ice phase frequencies compared with 100-km observations (Figure 3 h and l). However, in the NH, the model underestimates ice phase frequency and overestimates liquid phase frequencies from -30 to 0°C.

Smaller model biases are seen for mixed phase frequencies when compared with the 100-km observations, especially for the SH (Figure 3 h). However, the model still overestimates mixed phase frequency at -30 to -15°C and underestimates it at -15 to 0°C in the NH. In addition, the model misses the trend of increasing mixed phase frequencies at higher temperatures as shown by the observations. The results from Figures 2 and 3 indicate that the model biases in terms of phase occurrence frequency are more severe in the NH, consistent with the SLF biases in Figure 1.

3.3 Hemispheric comparisons of cloud microphysical properties in respective cloud phases

Cloud microphysical properties, i.e., LWC and IWC, are examined for individual cloud phase or all phases at various temperatures (Figure 4 a – h) alongside their hemispheric differences (i.e., NH minus SH) in Figure 4 i – p. The number of the samples is shown in Figure S8. Due to the definitions of three cloud phases, each phase may contain a certain amount of IWC, LWC, or both.

Focusing on the dominate type of hydrometeor in the liquid and ice phases, both observations show higher LWC of the liquid phase in the SH than NH (Figure 4 a) and relatively similar IWC of ice phase between the two hemispheres (Figure 4 g). Spatial averaging leads to higher decreases of LWC in liquid phase (Figure 4 a) and smaller decreases of IWC in ice phase (Figure 4 g) because most of the liquid segments are shorter than ice segments (not shown). More significant decreases of LWC are seen in the NH than SH after averaging, consistent with the more extensive coverage of supercooled liquid clouds over the SH as reported by previous studies (e.g., Hu et al., 2010; Desai et al., 2023, 2025; Barone et al., 2024).

Compared with 100-km observations, EAMv1 significantly overestimates the LWC in the liquid phase (Figure 4 a) and mixed phase (Figure 4 b), as well as overestimating the total LWC of all phases (Figure 4 d) by 1 – 2 orders of magnitude. In fact, the simulated LWC is closer to the 1-s observations than the 100-km observations. The overestimations of simulated LWC in both hemispheres lead to small hemispheric differences of LWC at -25 to -10°C, similar to the 100-km observations at that temperature range (Figure 4 l). At temperatures above -10°C, both observations show higher total LWC in the SH than NH, but the model shows the opposite hemispheric difference.

Differing from the consistent overestimation of LWC in all phases, the model biases in IWC vary with phase. The simulated total IWC of all phases is more similar to the 100-km observations except for the large negative biases in the NH around -20 to -5°C (Figure 4 h). However, the simulations overestimate IWC for mixed phase in two hemispheres (Figure 4 f) and underestimate IWC for ice phase in the SH (Figure 4 g). Despite these IWC biases for individual phase, the hemispheric differences in the total IWC (Figure 4 p) show similar results between EAMv1 and 100-km observations at -30 to -20°C with higher total IWC in the NH. However, EAMv1 misses the higher total IWC in the NH at -20 to 0°C due to its underestimation of the total IWC in the NH at that temperature range (Figure 4 h).

4. Discussions and Implications

A near global-scale dataset was compiled from 14 aircraft-based field campaigns, covering a wide latitudinal range from 75°S to 87°N. Distinct hemispheric differences were found based on *in situ* observations at various horizontal resolutions (i.e., 0.2 and 100 km), including higher SLF (Figure 1), higher liquid phase frequencies (Figures 2 and 3), and higher LWC in liquid phase (Figure 4) in the SH compared with the NH. All of these hemispheric differences are not represented in the EAMv1 simulations. Although previous studies also reported ubiquitous low-level marine boundary clouds with large spatial extent and significant amount of supercooled liquid water in the Southern Ocean region (e.g., Mace et al., 2021; Yang et al., 2021; Desai et al., 2023; Wang et al., 2024; Barone et al., 2024), a hemispheric comparison has rarely been conducted using *in situ* airborne observations.

Phase partition was quantified by two parameters in this work – liquid phase frequency (related to spatial coverage) and SLF (related to mass concentrations). The fact that observations show higher values of both parameters in the SH suggests that the SH has more liquid-containing segments relative to ice-containing segments and also higher mass concentrations of supercooled liquid droplets relative to ice crystals. This is consistent with a previous study of Maciel et al. (2024), which shows that the increasing mass fraction of supercooled liquid water is positively correlated with the spatial expansion of liquid-containing segments. Airborne observations in this study have limited samples in high-latitudinal regions especially in the SH outside austral summer, which leads to a knowledge gap regarding seasonality of phase partition in these regions. Previous satellite observations showed that the probability of supercooled liquid clouds as a function of mid-layer cloud temperature is not significantly different among various seasons as long as temperature is considered in the analysis (Hu et al., 2010). Future work is recommended to further investigate seasonality by leveraging recent observations, e.g., NASA Plankton, Aerosol, Cloud, ocean Ecosystem (PACE) and EU Earth Cloud Aerosol and Radiation Explorer (EarthCARE) missions.

We further diagnose the potential reasons behind the lack of hemispheric differences in EAMv1 by comparing against 100-km observations. The simulated ice phase frequencies in the

NH are lower by 0.1–0.2, while the SH shows more comparable values (Figure 3 l). These biases become even larger at the NH high latitudes since the observed ice phase frequencies further increase in that region (Figure 3 i and 3 j). The simulated LWC shows positive biases in both hemispheres (Figure 4 a, b, and d), while the simulated IWC in ice phase shows negative biases in the SH and comparable values in NH (Figure 4 g). Overall, the model biases associated with ice processes are more complex, compared with the consistent positive biases in LWC across all phases in both hemispheres. The model biases are likely attributed to EAMv1 model's treatments of ice nucleation and secondary ice production (SIP). EAMv1 uses the classical nucleation theory for ice nucleation, which severely underestimates concentrations of ice nucleating particles (INPs) in the NH high latitudes compared with DeMott et al. (2015) at -20°C – 0°C. The model also does not include high-latitude dust and biological INPs, which likely leads to low ice phase frequency, high LWC, and high SLF biases in the NH high latitudes. The lack of treatment of SIP and the uncertainties in droplet autoconversion may also lead to overestimations of LWC (Zhao et al., 2023).

Overall, this study provides a unique approach to examine phase partition at near global scale by compiling a large dataset based on *in situ* airborne observations, benefiting from an increasing number of flight campaigns over the high latitudes. The results indicate that by quantifying different properties of clouds (i.e., occurrence frequencies, phase partition, LWC and IWC in each phase), a model evaluation framework can be developed to diagnose the key processes contributing to model biases. In addition, this study demonstrates the feasibility of using high-resolution *in situ* observations to evaluate coarser-scale model simulations through scale-aware comparisons, as well as the potential usage of multiple flight campaigns for a near global-scale analysis. Lastly, the results from this study suggest that asymmetric distributions of ice and supercooled liquid water in the two hemispheres may lead to asymmetric responses of cloud radiative effects to a changing climate, which may potentially be overlooked if such hemispheric asymmetry in phase partition is not captured by model simulations.

Acknowledgements

Yang and Diao acknowledge funding from NSF AGS 1642291 and OPP 1744965, and DOE RDPP DE-SC0023155 and CRC DESC0024439. Diao acknowledges NASA PACE Grant 80NSSC24K1616. All authors acknowledge DOE ASR Grant DE-SC0021211. We acknowledge the support from the field campaign science team and helpful comments regarding aircraft-based observations from Dr. Aaron Bansemer at NSF NCAR and Drs. Fan Mei and Beat Schmidt at DOE PNNL. This research used resources of the DOE National Energy Research Scientific Computing Center (NERSC) under awards BER-ERCAP0019880, ERCAP0025013, ERCAP0032053, and ERCAP0032052.

Open Research

Airborne observations are publicly accessible for 11 NSF campaigns (UCAR/NCAR, 2018a, b, 2019a–f, 2020, 2021a, b, 2022a–c) and 3 DOE campaigns (DOE ARM 2024 a, b, c). Key variables of the EAMv1 nudged simulations are stored in an open archive (Yang et al., 2024).

References

Abdi, D. S., Giraldo, F. X., Constantinescu, E. M., Carr, L. E., Wilcox, L. C., & Warburton, T. C. (2017). Acceleration of the IMplicit-EXplicit nonhydrostatic unified model of the atmosphere on manycore processors. *The International Journal of High Performance Computing Applications*, *0*(0), 1094342017732395. https://doi.org/10.1177/1094342017732395

Albrecht, B., Ghate, V., Mohrmann, J., Wood, R., Zuidema, P., Bretherton, C., et al. (2019). Cloud System Evolution in the Trades (CSET): Following the Evolution of Boundary Layer Cloud Systems with the NSF–NCAR GV. *Bulletin of the American Meteorological Society*, *100*(1), 93–121. https://doi.org/10.1175/BAMS-D-17-0180.1

Barone, T., Diao, M., Shi, Y., Zhao, X., Liu, X., & Silber, I. (2024). Impacts of Synoptic-Scale Dynamics on Clouds and Radiation in High Southern Latitudes. *Journal of Geophysical Research: Atmospheres*, *129*(16). https://doi.org/10.1029/2023JD040329

Barth, M. C., Cantrell, C. A., Brune, W. H., Rutledge, S. A., Crawford, J. H., Huntrieser, H., et al. (2015). The Deep Convective Clouds and Chemistry (DC3) Field Campaign. *Graduate School of Oceanography Faculty Publications*, *96*(8), 1281–1310. https://doi.org/10.1175/BAMS-D-13-00290.1

Brown, P. R. A., & Francis, P. N. (1995). Improved measurements of the ice water content in cirrus using a total-water probe. Journal of Atmospheric and Oceanic Technology, 12(2), 410–414. https://doi.org/10.1175/1520-0426(1995)012<0410:IMOTIW>2.0.CO;2

Cesana, G., Chepfer, H., Winker, D., Getzewich, B., Cai, X., Jourdan, O., et al. (2016). Using in situ airborne measurements to evaluate three cloud phase products derived from CALIPSO. *Journal of Geophysical Research: Atmospheres*, *121*(10), 5788–5808. https://doi.org/10.1002/2015JD024334

Cesana, G., Khadir, T., Chepfer, H., & Chiriaco, M. (2022). Southern Ocean Solar Reflection Biases in CMIP6 Models Linked to Cloud Phase and Vertical Structure Representations. *Geophysical Research Letters*, *49*(22). https://doi.org/10.1029/2022GL099777

D'Alessandro, J. J., M. Diao, C. Wu, X. Liu, J. B. Jensen, and B. B. S. (2019). Cloud Phase and Relative Humidity Distributions over the Southern Ocean in Austral Summer Based on In Situ Observations and CAM5 Simulations. *J. Climate*, *32*, 2781–2805. https://doi.org/https://doi.org/10.1175/JCLI-D-18-0232.1

D'Alessandro, J. J., McFarquhar, G. M., Stith, J. L., Diao, M., DeMott, P. J., McCluskey, C. S., et al. (2023). An evaluation of phase, aerosol-cloud interactions and microphysical properties of single- and multi-layer clouds over the Southern Ocean using in situ observations from SOCRATES. *Journal of Geophysical Research: Atmospheres*, 128, e2023JD038610. https://doi.org/10.1029/2023JD038610

DeMott, P. J., Prenni, A. J., McMeeking, G. R., Sullivan, R. C., Petters, M. D., Tobo, Y., Niemand, M., Möhler, O., Snider, J. R., Wang, Z., and Kreidenweis, S. M. (2015). Integrating laboratory and field data to quantify the immersion freezing ice nucleation activity of mineral dust particles, *Atmos. Chem. Phys.*, 15, 393–409, https://doi.org/10.5194/acp-15-393-2015

Dennis, J. M., Edwards, J., Evans, K. J., Guba, O., Lauritzen, P. H., Mirin, A. A., et al. (2012). CAM-SE: A scalable spectral element dynamical core for the Community Atmosphere Model. *International Journal of High Performance Computing*, *26*(1), 74–89. https://doi.org/10.1177/1094342011428142

Desai, N., Diao, M., Shi, Y., Liu, X., & Silber, I. (2023). Ship-Based Observations and Climate Model Simulations of Cloud Phase Over the Southern Ocean. *Journal of Geophysical Research: Atmospheres*, *128*(11). https://doi.org/10.1029/2023jd038581

Desai, N., Diao, M., Shi, Y., & Liu, X. (2025). A comparative study of cloud properties between northern and southern high latitudes based on ARM observations and EAMv2 simulations. *Journal of Geophysical Research: Atmospheres*, 130, e2024JD041588. https://doi.org/10.1029/2024JD041588

DOE ARM. (2024a). ACME-V campaign [Dataset]. https://www.arm.gov/research/campaigns/aaf2015armacmev

DOE ARM. (2024b). ISDAC campaign [Dataset]. https://www.arm.gov/research/campaigns/aaf2008isdac

DOE ARM. (2024c). M-PACE campaign [Dataset]. https://www.arm.gov/research/campaigns/nsa2004arcticcldFrey, W. R., & Kay, J. E. (2017). The influence of extratropical cloud phase and amount feedbacks on climate sensitivity. *Climate Dynamics*, 1–20. https://doi.org/10.1007/s00382-017-3796-5

Fuchs-Stone, Raymond, D. J., & Sentić, S. (2020). OTREC2019: Convection Over the East Pacific and Southwest Caribbean. *Geophysical Research Letters*, *47*(11), e2020GL087564. https://doi.org/10.1029/2020GL087564

Gelaro, R., and Coauthors. (2017). The Modern-Era Retrospective Analysis for Research and Applications, Version 2 (MERRA-2). *J. Climate*, 30, 5419–5454, https://doi.org/10.1175/JCLI-D-16-0758.1.

Gettelman, A., & Morrison, H. (2015). Advanced two-moment bulk microphysics for global models. Part I: Off-line tests and comparison with other schemes. *Journal of Climate*, *28*(3), 1268–1287. https://doi.org/10.1175/JCLI-D-14-00102.1

Golaz, J. C., Caldwell, P. M., Van Roekel, L. P., Petersen, M. R., Tang, Q., Wolfe, J. D., et al. (2019). The DOE E3SM Coupled Model Version 1: Overview and Evaluation at Standard Resolution. *Journal of Advances in Modeling Earth Systems*, *11*(7). https://doi.org/10.1029/2018MS001603

Golaz, J. C., Larson, V. E., & Cotton, W. R. (2002). A PDF-based model for boundary layer clouds. Part I: Method and model description. *Journal of the Atmospheric Sciences*, *59*(24). https://doi.org/10.1175/1520-0469(2002)059<3540:APBMFB>2.0.CO;2

Hartmann, D. L., Ockert-Bell, M. E., & Michelsen, M. L. (1992). The Effect of Cloud Type on Earth's Energy Balance: Global Analysis. *Journal of Climate*, *5*(11). https://doi.org/10.1175/1520-0442(1992)005<1281:teocto>2.0.co;2

Hofer, S., Hahn, L. C., Shaw, J. K., McGraw, Z. S., Bruno, O., Hellmuth, F., et al. (2024). Realistic representation of mixed-phase clouds increases projected climate warming. *Communications Earth and Environment*, *5*(390). https://doi.org/10.1038/s43247-024-01524-2

Hogan, R. J., Gaussiat, N., & Illingworth, A. J. (2005). Stratocumulus liquid water content from dual-wavelength radar. *Journal of Atmospheric and Oceanic Technology*, *22*(8). https://doi.org/10.1175/JTECH1768.1

Hu, Y., S. Rodier, K. Xu, W. Sun, J. Huang, B. Lin, P. Zhai, and D. Josset (2010), Occurrence, liquid water content, and fraction of supercooled water clouds from combined CALIOP/IIR/MODIS measurements, *J. Geophys. Res.*, *115*, D00H34, doi:10.1029/2009JD012384.

Jackson, R. C., G. M. McFarquhar, A. V. Korolev, M. E. Earle, P. S. K. Liu, R. P. Lawson, S. Brooks, M. Wolde, A. Laskin, and M. Freer (2012), The dependence of ice microphysics on aerosol concentration in arctic mixed-phase stratus clouds during ISDAC and M-PACE, *J. Geophys. Res.*, 117, D15207, doi:10.1029/2012JD017668.

Kay, J. E., Bourdages, L., Miller, N. B., Morrison, A., Yettella, V., Chepfer, H., & Eaton, B. (2016). Evaluating and improving cloud phase in the Community Atmosphere Model version 5 using spaceborne lidar observations. *Journal of Geophysical Research: Atmospheres*, *121*(8), 4162–4176. https://doi.org/10.1002/2015JD024699

Korolev, A. V., McFarquhar, G., Field, P. R., Franklin, C., Lawson, P., Wang, Z., et al. (2017). Mixed-Phase Clouds: Progress and Challenges. *Meteorological Monographs*, *58*, 5.1–5.50, https://doi.org/10.1175/amsmonographs-d-17-0001.1

Korolev, A. V., & Milbrandt, J. (2022). How Are Mixed-Phase Clouds Mixed? *Geophysical Research Letters*, *49*(18), 1–7. https://doi.org/10.1029/2022GL099578

Larson, V. E., & Golaz, J. C. (2005). Using probability density functions to derive consistent closure relationships among higher-order moments. *Monthly Weather Review*, *133*(4). https://doi.org/10.1175/MWR2902.1

Lee, B. H., Lopez-Hilfiker, F. D., Schroder, J. C., Campuzano-Jost, P., Jimenez, J. L., McDuffie, E. E., et al. (2018). Airborne Observations of Reactive Inorganic Chlorine and Bromine Species in the Exhaust of Coal-Fired Power Plants. *Journal of Geophysical Research: Atmospheres*, *123*(19), 11,225-11,237. https://doi.org/10.1029/2018JD029284

Liu, X., Ma, P. L., Wang, H., Tilmes, S., Singh, B., Easter, R. C., et al. (2016). Description and evaluation of a new four-mode version of the Modal Aerosol Module (MAM4) within version 5.3 of the Community Atmosphere Model. *Geoscientific Model Development*, *9*(2), 505–522. https://doi.org/10.5194/gmd-9-505-2016

Maahn, M., De Boer, G., Creamean, J. M., Feingold, G., McFarquhar, G. M., Wu, W., & Mei, F. (2017). The observed influence of local anthropogenic pollution on northern Alaskan cloud properties. *Atmospheric Chemistry and Physics*, *17*(23). https://doi.org/10.5194/acp-17-14709-2017

Mace, G. G., Protat, A., & Benson, S. (2021). Mixed-Phase Clouds Over the Southern Ocean as Observed From Satellite and Surface Based Lidar and Radar. *Journal of Geophysical Research: Atmospheres*, *126*(16), e2021JD034569. https://doi.org/10.1029/2021JD034569

Maciel, F. V., Diao, M., & Yang, C. A. (2024). Partition between Supercooled Liquid Droplets and Ice Crystals in Mixed-phase Clouds based on Airborne In-situ Observations. *Atmospheric Measurement Techniques*, *17*(16), 4843–4861. https://doi.org/https://doi.org/10.5194/amt-17-4843-2024

Matus, A. V., & L'Ecuyer, T. S. (2017). The role of cloud phase in Earth's radiation budget. *Journal of Geophysical Research*, *122*(5), 2559–2578. https://doi.org/10.1002/2016JD025951

McCoy, I. L., Wood, R., & Fletcher, J. K. (2017). Identifying Meteorological Controls on Open and Closed Mesoscale Cellular Convection Associated with Marine Cold Air Outbreaks. *Journal of Geophysical Research: Atmospheres*, *122*(21). https://doi.org/10.1002/2017JD027031

McFarquhar, G. M., Bretherton, C. S., Marchand, R., Protat, A., DeMott, P. J., Alexander, S. P., et al. (2021). Observations of clouds, aerosols, precipitation, and surface radiation over the southern ocean. *Bulletin of the American Meteorological Society*, *102*(4), E894–E928. https://doi.org/10.1175/BAMS-D-20-0132.1

McFarquhar, G. M., Ghan, S., Verlinde, J., Korolev, A., Strapp, J. W., Schmid, B., et al. (2011). Indirect and Semi-direct Aerosol Campaign: The Impact of Arctic Aerosols on Clouds. *Bulletin of the American Meteorological Society*, *92*(2), 183–201. https://doi.org/10.1175/2010BAMS2935.1

McFarquhar, G. M., Zhang, G., Poellot, M. R., Kok, G. L., McCoy, R., Tooman, T., et al. (2007). Ice properties of single-layer stratocumulus during the Mixed-Phase Arctic Cloud Experiment: 1. Observations. *Journal of Geophysical Research: Atmospheres*, *112*(D24), 24201. https://doi.org/10.1029/2007JD008633

Montgomery, M. T., Davis, C., Dunkerton, T., Wang, Z., Velden, C., Torn, R., et al. (2012). The Pre-Depression Investigation of Cloud-Systems in the Tropics (PREDICT) Experiment: Scientific Basis, New Analysis Tools, and Some First Results. *Bulletin of the American Meteorological Society*, *93*(2), 153–172. https://doi.org/10.1175/BAMS-D-11-00046.1

Pan, L. L., Atlas, E. L., Salawitch, R. J., Honomichl, S. B., Bresch, J. F., Randel, W. J., et al. (2017). The convective transport of active species in the tropics (Contrast) experiment. *Bulletin of the American Meteorological Society*, *98*(1). https://doi.org/10.1175/BAMS-D-14-00272.1

Pan, L. L., Bowman, K. P., Atlas, E. L., Wofsy, S. C., Zhang, F., Bresch, J. F., et al. (2010). The Stratosphere–Troposphere Analyses of Regional Transport 2008 Experiment. *Bulletin of the American Meteorological Society*, *91*(3), 327–342. https://doi.org/10.1175/2009BAMS2865.1

Patnaude, R. J., Moore, K. A., Perkins, R. J., Hill, T. C. J., Demott, P. J., & Kreidenweis, S. M. (2024). Low-temperature ice nucleation of sea spray and secondary marine aerosols under cirrus cloud conditions. *Atmospheric Chemistry and Physics*, *24*(2). https://doi.org/10.5194/acp-24-911-2024

Rasch, P. J., S. Xie, P.-L. Ma, W. Lin, H. Wang, Q. Tang, S. M. Burrows, P. Caldwell, K. Zhang, R. C. Easter, et al. (2019), An Overview of the Atmospheric Component of the Energy Exascale Earth System Model, *J. Adv. Model. Earth Syst.*, 11, 2377–2411, https://doi.org/10.1029/2019MS001629.

Silber, I., Verlinde, J., Eloranta, E. W., & Cadeddu, M. (2018). Antarctic cloud macrophysical, thermodynamic phase, and atmospheric inversion coupling properties at McMurdo station: I. principal data processing and climatology. *Journal of Geophysical Research: Atmospheres*, 123(11), 6099–6121. https://doi.org/10.1029/2018JD028279

Sokol, A. B., & Storelvmo, T. (2024). The Spatial Heterogeneity of Cloud Phase Observed by Satellite. *Journal of Geophysical Research: Atmospheres*, *129*(3). https://doi.org/10.1029/2023JD039751

Stephens, B. B., Long, M. C., Keeling, R. F., Kort, E. A., Sweeney, C., Apel, E. C., et al. (2018). The O2/N2 Ratio and CO2 Airborne Southern Ocean Study. *Bulletin of the American Meteorological Society*, *99*(2), 381–402. https://doi.org/10.1175/BAMS-D-16-0206.1

Tan, I., & Storelvmo, T. (2016). Sensitivity study on the influence of cloud microphysical parameters on mixed-phase cloud thermodynamic phase partitioning in CAM5. *Journal of the Atmospheric Sciences*, *73*(2), 709–728. https://doi.org/10.1175/JAS-D-15-0152.1

Tan, I., Storelvmo, T., & Zelinka, M. D. (2016). Observational constraints on mixed-phase clouds imply higher climate sensitivity. *Science*, *352*(6282), 224–227. https://doi.org/10.1126/SCIENCE.AAD5300/SUPPL_FILE/AAD5300-TAN-SM.PDF

UCAR/NCAR - Earth Observing Laboratory. (2018a). DC3: Low Rate (LRT - 1 sps) Navigation, State Parameter, and Microphysics Flight-Level Data (NetCDF). Version 3.0. UCAR/NCAR - Earth Observing Laboratory. [Dataset] https://doi.org/10.5065/D6BC3WKB. Accessed 28 Feb 2025.

UCAR/NCAR - Earth Observing Laboratory. (2018b). ORCAS: Low Rate (LRT - 1 sps) Navigation, State Parameter, and Microphysics Flight-Level Data. Version 1.1.

UCAR/NCAR - Earth Observing Laboratory. [Dataset]. https://doi.org/10.5065/D65T3HWR. Accessed 28 Feb 2025.

UCAR/NCAR - Earth Observing Laboratory. (2019a). HIPPO2: Low Rate (LRT - 1 sps) Navigation, State Parameter, and Microphysics Flight-Level Data. Version 5.0. UCAR/NCAR - Earth Observing Laboratory. [Dataset]. https://doi.org/10.5065/D6JW8C64. Accessed 28 Feb 2025.

UCAR/NCAR - Earth Observing Laboratory. (2019b). HIPPO3: Low Rate (LRT - 1 sps) Navigation, State Parameter, and Microphysics Flight-Level Data. Version 5.0. UCAR/NCAR - Earth Observing Laboratory. [Dataset]. https://doi.org/10.5065/D6QF8R6R. Accessed 28 Feb 2025.

UCAR/NCAR - Earth Observing Laboratory. (2019c). HIPPO4: Low Rate (LRT - 1 sps) Navigation, State Parameter, and Microphysics Flight-Level Data. Version 3.0. UCAR/NCAR - Earth Observing Laboratory. [Dataset]. https://doi.org/10.5065/D6V40SK6. Accessed 28 Feb 2025.

UCAR/NCAR - Earth Observing Laboratory. (2019d). HIPPO5: Low Rate (LRT - 1 sps) Navigation, State Parameter, and Microphysics Flight-Level Data. Version 3.0. UCAR/NCAR - Earth Observing Laboratory. [Dataset]. https://doi.org/10.5065/D6CZ35HX. Accessed 28 Feb 2025.

UCAR/NCAR - Earth Observing Laboratory. (2019e). START08: Low Rate (LRT - 1 sps) Navigation, State Parameter, and Microphysics Flight-Level Data. Version 2.0. UCAR/NCAR - Earth Observing Laboratory. [Dataset]. https://doi.org/10.5065/D6NZ85Z4. Accessed 28 Feb 2025.

UCAR/NCAR - Earth Observing Laboratory. (2019f). TORERO: Low Rate (LRT - 1 sps) Navigation, State Parameter, and Microphysics Flight-Level Data. Version 3.0. UCAR/NCAR - Earth Observing Laboratory. [Dataset]. https://doi.org/10.5065/D6668BHR. Accessed 28 Feb 2025.

UCAR/NCAR - Earth Observing Laboratory. (2020). OTREC: Low Rate (LRT - 1 sps) Navigation, State Parameter, and Microphysics Flight-Level Data. Version 1.0. UCAR/NCAR - Earth Observing Laboratory. [Dataset]. https://doi.org/10.26023/DTDS-MPYV-CT0R. Accessed 28 Feb 2025.

UCAR/NCAR - Earth Observing Laboratory. (2021a). CONTRAST: Low Rate (LRT - 1 sps) Navigation, State Parameter, and Microphysics Flight-Level Data. Version 1.3. UCAR/NCAR - Earth Observing Laboratory. [Dataset]. https://doi.org/10.5065/D6TX3CK0. Accessed 28 Feb 2025.

UCAR/NCAR - Earth Observing Laboratory. (2021b). PREDICT: Low Rate (LRT - 1 sps) Navigation, State Parameter, and Microphysics Flight-Level Data. Version 3.0. UCAR/NCAR - Earth Observing Laboratory. [Dataset]. https://doi.org/10.5065/D61R6NV5. Accessed 28 Feb 2025.

UCAR/NCAR - Earth Observing Laboratory. (2022a). CSET: Low Rate (LRT - 1 sps) Navigation, State Parameter, and Microphysics Flight-Level Data. Version 1.4. UCAR/NCAR - Earth Observing Laboratory. [Dataset]. https://doi.org/10.5065/D65Q4T96. Accessed 28 Feb 2025.

UCAR/NCAR - Earth Observing Laboratory. (2022b). SOCRATES: Low Rate (LRT - 1 sps) Navigation, State Parameter, and Microphysics Flight-Level Data. Version 1.4. UCAR/NCAR - Earth Observing Laboratory. [Dataset]. https://doi.org/10.5065/D6M32TM9. Accessed 28 Feb 2025.

UCAR/NCAR - Earth Observing Laboratory. (2022c). WINTER: Low Rate (LRT - 1 sps) Navigation, State Parameter, and Microphysics Flight-Level Data. Version 1.2. UCAR/NCAR - Earth Observing Laboratory. [Dataset]. https://doi.org/10.5065/D68C9TB1. Accessed 28 Feb 2025.

Verlinde, J., Harrington, J. Y., McFarquhar, G. M., Yannuzzi, V. T., Avramov, A., Greenberg, S., et al. (2007). The Mixed-Phase Arctic Cloud Experiment. *Bulletin of the American Meteorological Society*, *88*(2), 205–222. https://doi.org/10.1175/BAMS-88-2-205

Volkamer, R., Baidar, S., Campos, T. L., Coburn, S., DiGangi, J. P., Dix, B., et al. (2015). Aircraft measurements of BrO, IO, glyoxal, NO2, H2O, O2-O2 and aerosol extinction profiles in the tropics: Comparison with aircraft-/ship-based in situ and lidar measurements. *Atmospheric Measurement Techniques*, *8*(5), 2121–2148. https://doi.org/10.5194/AMT-8-2121-2015

Wang, D., Yang, C. A., & Diao, M. (2024). Validation of Satellite-Based Cloud Phase Distributions Using Global-Scale In Situ Airborne Observations. *Earth and Space Science*, *11*(5), e2023EA003355. https://doi.org/10.1029/2023EA003355

Wofsy, S. C. (2011). HIAPER Pole-to-Pole Observations (HIPPO): fine-grained, global-scale measurements of climatically important atmospheric gases and aerosols. *Philosophical Transactions of the Royal Society A: Mathematical, Physical and Engineering Sciences*, *369*(1943), 2073–2086. https://doi.org/10.1098/RSTA.2010.0313

Xie, S., Lin, W., Rasch, P. J., Ma, P.-L., Neale, R., Larson, V. E., et al. (2018). Understanding cloud and convective characteristics in version 1 of the E3SM atmosphere model. *Journal of Advances in Modeling Earth Systems*, 10, 2618–2644. https://doi.org/10.1029/2018MS001350

Yang, C. A., Diao, M., Gettelman, A., Zhang, K., Sun, J., McFarquhar, G., & Wu, W. (2021). Ice and Supercooled Liquid Water Distributions Over the Southern Ocean Based on In Situ Observations and Climate Model Simulations. *Journal of Geophysical Research: Atmospheres*, *126*(24). https://doi.org/10.1029/2021JD036045

Yang, C. A., Diao, M., Yang, S., & Liu, X. (2024). EAMv1 for Yang et al. (2024). [Dataset]. Mendeley Data, V1, https://doi.org/10.17632/db4vbfrn2z.1

Yip, J., Diao, M., Barone, T., Silber, I., & Gettelman, A. (2021). Evaluation of the CAM6 Climate Model Using Cloud Observations at McMurdo Station, Antarctica. *Journal of Geophysical Research: Atmospheres*, *126*(16), e2021JD034653. https://doi.org/10.1029/2021JD034653

Zelinka, M. D., Myers, T. A., McCoy, D. T., Po-Chedley, S., Caldwell, P. M., Ceppi, P., et al. (2020). Causes of Higher Climate Sensitivity in CMIP6 Models. *Geophysical Research Letters*, *47*(1). https://doi.org/10.1029/2019GL085782

Zhang, G. J., & McFarlane, N. A. (1995). Sensitivity of climate simulations to the parameterization of cumulus convection in the Canadian climate centre general circulation model. *Atmosphere - Ocean*, *33*(3). https://doi.org/10.1080/07055900.1995.9649539

Zhang, M., Liu, X., Diao, M., D’Alessandro, J. J., Wang, Y., Wu, C., et al. (2019). Impacts of Representing Heterogeneous Distribution of Cloud Liquid and Ice on Phase Partitioning of Arctic Mixed-Phase Clouds with NCAR CAM5. *Journal of Geophysical Research: Atmospheres*, *124*(23), 13071–13090. https://doi.org/10.1029/2019JD030502

Zhang, Y., Xie, S., Qin, Y., Lin, W., Golaz, J.-C., Zheng, X., Ma, P.-L., Qian, Y., Tang, Q., Terai, C. R., and Zhang, M. (2024). Understanding changes in cloud simulations from

E3SM version 1 to version 2, *Geosci. Model Dev.*, 17, 169–189, https://doi.org/10.5194/gmd-17-169-2024.

Zhao, X., Liu, X., Burrows, S., DeMott, P. J., Diao, M., McFarquhar, G. M., et al. (2023). Important ice processes are missed by the Community Earth System Model in Southern Ocean mixed-phase clouds: Bridging SOCRATES observations to model developments. *Journal of Geophysical Research: Atmospheres*, 128, e2022JD037513. https://doi.org/10.1029/2022JD037513

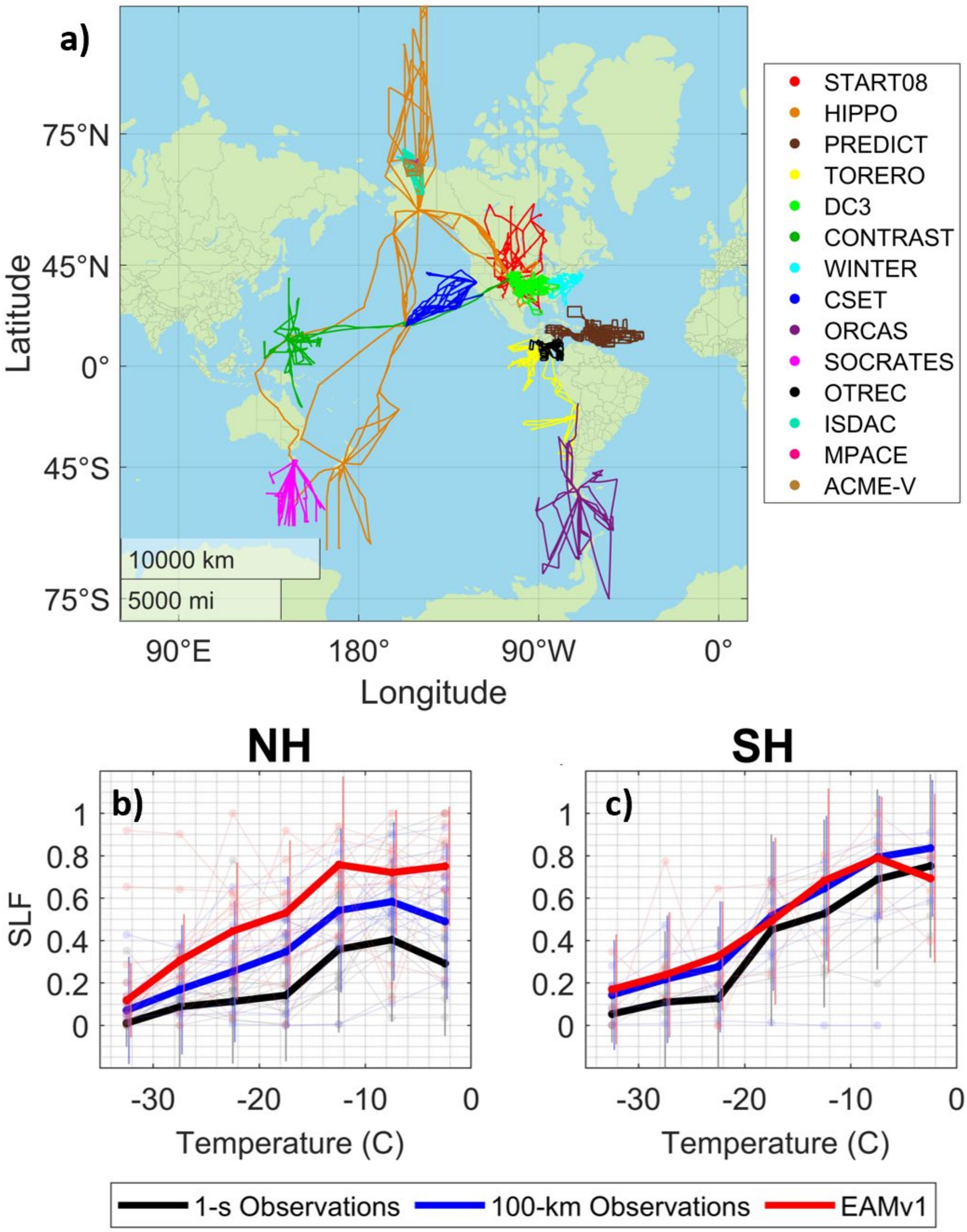

Figure 1. (a) Flight tracks of 11 NSF and 3 DOE campaigns. Supercooled liquid fraction (SLF) averaged by 5°C bins in the (b) NH and (c) SH. The average SLF of individual campaigns is shown in light colored dots. Vertical bars represent standard deviations of all campaigns.

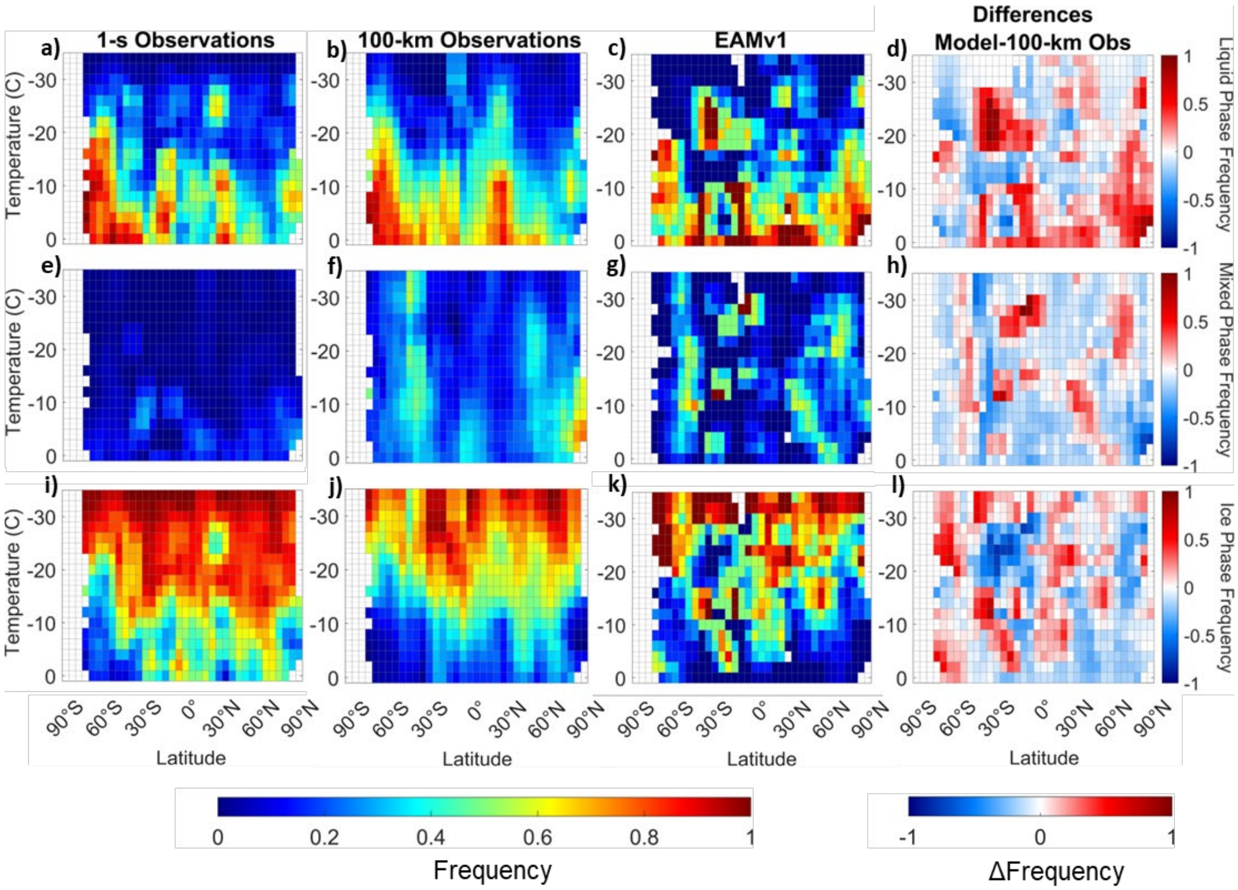

609

610 **Figure 2**. Occurrence frequencies of (a–c) liquid, (e–g) mixed, and (i–k) ice phase in a latitude-
611 temperature view. (d, h, l) Differences of model and 100-km observations.

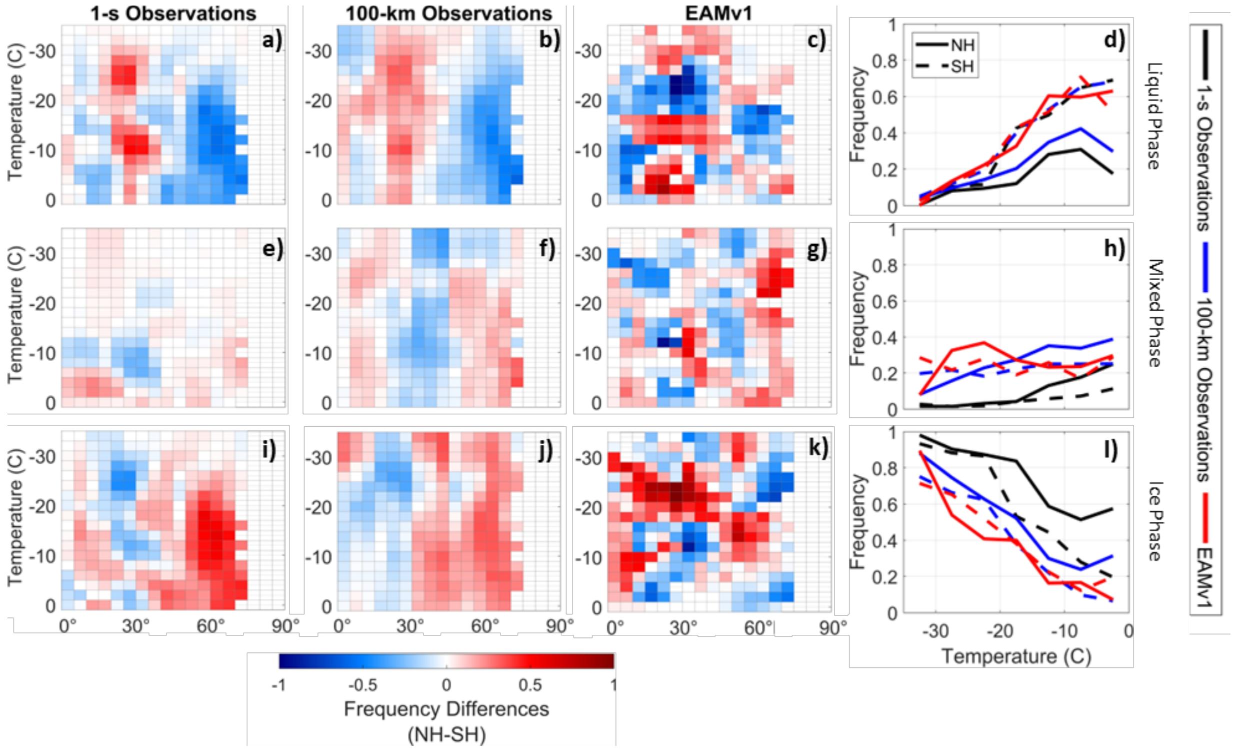

Figure 3. Hemispheric differences (NH minus SH) of occurrence frequencies for (a–c) liquid, (e–g) mixed, and (i–k) ice phase. The last column shows the average cloud phase frequencies in each 5°C bin.

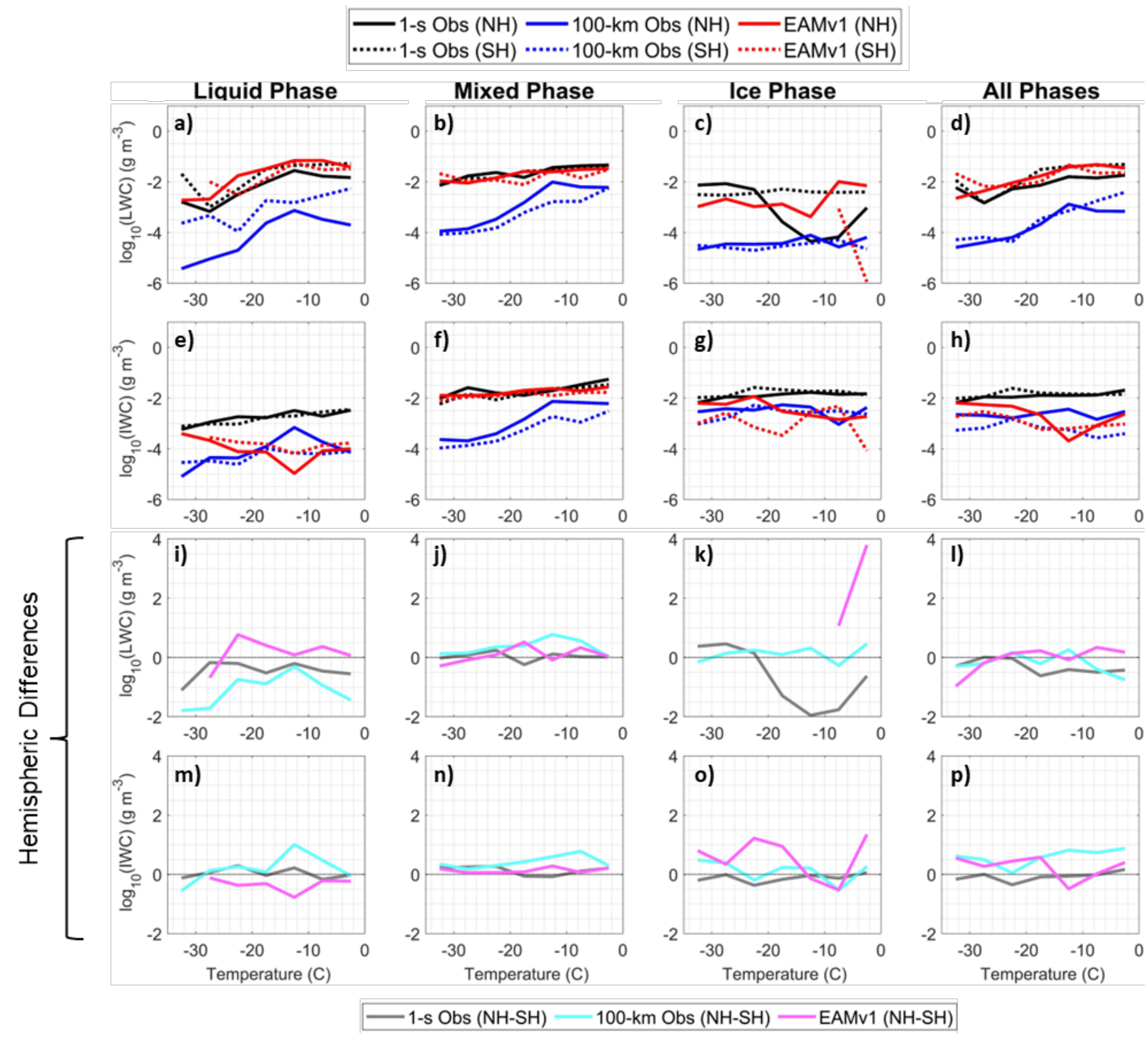

Figure 4. Average values of (a–d) LWC and (e–h) IWC for liquid, mixed, ice phase, and all phases (columns 1 to 4, respectively). Hemispheric differences for (i–l) LWC and (m–p) IWC.